Texas A&M University's AggieSat Laboratory

Synthetic Orbital Landing Area for Crater Elimination (SOLACE)

AggieSat Laboratory Faculty Advisor Helen Reed, Ph.D, P.E.

AggieSat Laboratory Program Manager Shirish Pandam, B.S. (G, AERO)

SOLACE Project Manager Kamalika Bose (UG, MXET)

SOLACE Chief Engineer Nicholas X. Siodlarz, B.S. (G, BUSI)

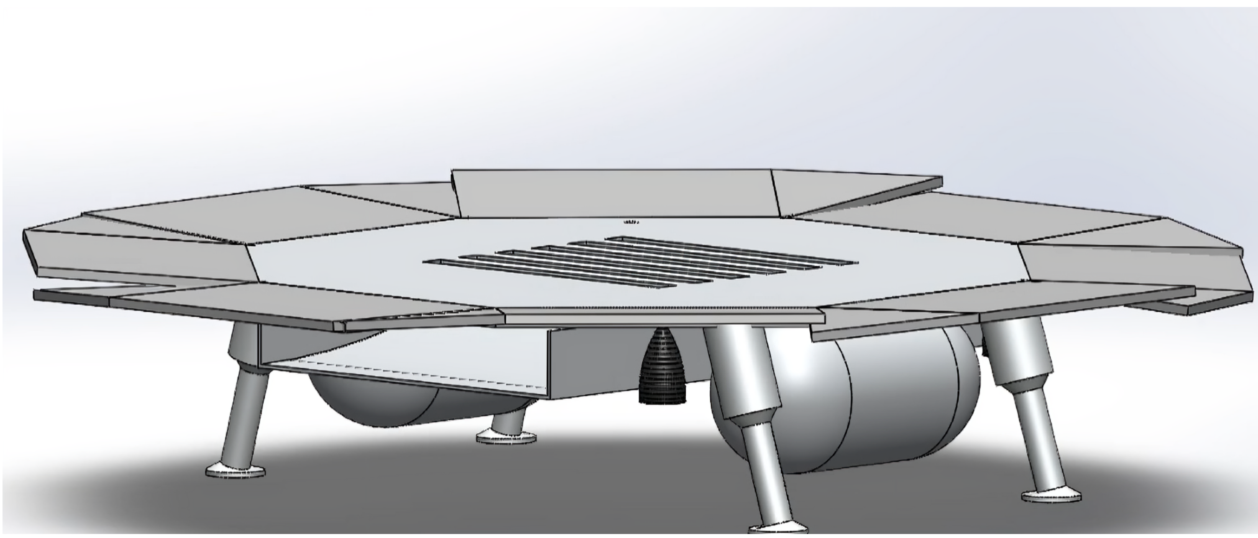

Faculty Advisor Signature: Helen L Reed

SOLACE Personnel

Command and Data Handling
Lead: Yusif El-awawdeh, (G, GEOG)
Brayden Hudson, (UG, ESET)
Aidan Jones, (UG, GENE)
Daniel Vinnik, (UG, ESET)

Communications
Lead: Thomas Honeywill, (G, ECEN)
Ayush Mishra, (UG, AERO)
Josh Wu, (UG, CPEN)

Electrical Power Subsystem
Lead: Thomas Lopez, (UG, ESET)
Kyle Carlson, (UG, ECEN)
Jaret Pinkerton, (UG, MXET)

Guidance, Navigation, and Control
Lead: Travis Mason, (UG, AERO)
Joseph Carbone, (UG, AERO)
Adam Knight, (UG, AERO)

Surface, Integration, and Test Environment
Lead: Akshyat Dumka, (UG, MXET)
Kai Elmore, (UG, AERO)
Abhinav Sivakumar, (UG, MXET)
Bao Tran, (UG, AERO)

Thermal, Mechanics, and Structures
Lead: Thomas Magee, (UG, AERO, PHYS)
Brandon Elliott, (UG, AERO)
Theresia Heimer, (UG, ITDE)
Pan Zhou, (UG, MEEN)

Key
UG -Undergraduate
G - Graduate

AERO - Aerospace Engineering
BUSI - Business
CPEN - Computer Engineering
ECEN - Electrical Engineering
ESET - Electronic Systems and Engineering Technologies
GEOG - Geography
ITDE - Interdisciplinary Engineering
MATH - Mathematics
MEEN - Mechanical Engineering
MXET - Mechatronics Engineering
PHYS - Physics

Texas A&M University – Synthetic Orbital Landing Area for Crater Elimination (SOLACE)

Major Objectives & Technical Approach

- Act as a safe landing platform for descent, landing, and ascent systems on the Moon
- Reduce cratering and the impact of regolith dispersion on local infrastructure for a timespan of 10 years
- Monitor PSI on descent and during future HLS landings
- The approach is to develop a landing pad that shall land on the Moon from LLO, withstand large temperature gradients, and redirect rocket plumes in a safe direction to reduce dispersion and cratering

Image/Graphic:.

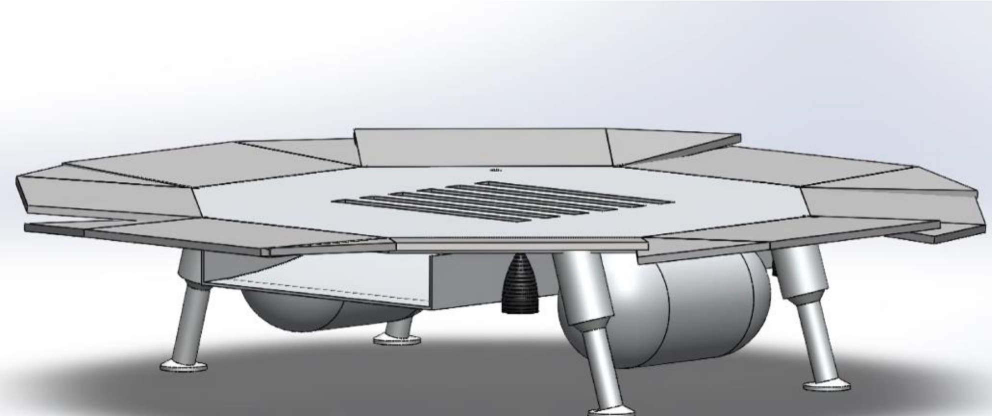

Key Design Details & Innovations of the Concept

- SOLACE shall consist of an octagonal platform with deployable fins, liquid-propelled boosters, landing legs, a plume redirection compartment, and an electronics safety box
- SOLACE shall contain LiDAR, cameras, accelerometers, and gyros among other sensors which can be used to measure PSI on descent in addition to their primary functions.
- SOLACE consists of a novel machine learning based guidance system, plume redirection system, and employs NASA's Navigational Doppler LiDAR (NDL), a relatively new LiDAR instrument.

Summary of Schedule & Costs for the proposed solution's path to adoption

- Major milestones in Design, Test, and Evaluation include
  - System assembly concludes – 2 years into DTE
  - Test and Evaluation concludes – 4.2 years into DTE
  - Launch – 4.5 years into DTE
- Costing of the mission was found to be $1944.9M
  - $290.5M for Non-Recurring Costs
  - $1051.8M for Recurring Production Costs
  - $189.9M for launch and $370.2M for operations

TABLE OF CONTENTS

NOMENCLATURE

AGSL	AggieSat Laboratory
BER	Bit Error Rate
BLDC	Brushless DC
CDH	Command and Data Handling
CONOPS	Concept of Operations
CSS	Coarse Sun Sensor
COM	Communications
DLA	Descent, Landing, and Ascent
DTE	Design, Test, and Evaluation
EPS	Electrical Power Subsystem
FEC	Forward Error Correction
FSM	Finite State Machine
GMAT	General Mission Analysis Toolkit
GNC	Guidance, Navigation, and Control
HLS	Human Landing System
HSM	Hierarchical State Machine
HuLC	Human Lander Challenge
IMU	Inertial Measurement Unit
LLO	Low Lunar Orbit
NASA	National Aeronautics and Space Administration
NDL	Navigational Doppler LiDAR
NIA	National Institute of Aerospace
NRC	Non-recurring Cost
PCEC	Project Cost Estimating Capability
PDU	Power Distribution Unit

PSI	Plume Surface Interaction
PSR	Permanently Shadowed Regions
PWM	Pulse Width Modulation
SOLACE	Synthetic Orbital Landing Area for Crater Elimination
SITE	Surface, Integration, and Test Environment
SLS	Space Launch System
TDRSS	Tracking and Data Relay Satellites
TMS	Thermal, Mechanics, and Structures
TRL	Technology Readiness Level
VV	Verification and Validation
WBS	Work Breakdown Structure

1. PSI-INDUCED LUNAR EROSION AND DISPERSAL

NASA, through its Human Lander Challenge (HuLC), identifies the importance and necessity of "innovative solutions addressing the mitigation of lunar Plume-Surface Interaction (PSI)" [1]. Particularly, it highlights two key categories of lunar PSI that should be studied in depth: cratering and ejecta production. In response to this challenge, AggieSat Laboratory (AGSL) has designed a system capable of mitigating the erosion and dispersal caused by lunar PSI, while also better characterizing the phenomenon itself.

1.1 Background

A major hindrance to future thrust-based descent, landing, and ascent (DLA) systems is the erosion of the lunar surface and production of high velocity ejecta during engine plume interaction with the lunar surface. Specifically, lunar surface erosion refers to the "cratering" of the landing site, altering the environment via the removal of local regolith, while ejecta refers to dust and rocks blown from the landing site at high speeds, at times exceeding lunar escape velocity [2, 3]. These phenomena pose technical and operational threats to landing systems. During the Apollo missions, ejecta thrown up during descent directly caused vision obscuration, false velocity readings due to sensors locking onto moving dust, and clogged mechanisms [5]. Specifically, during Apollo 12, Surveyor III was sandblasted on Apollo 12's descent, with visible evidence displayed in Figure 1 [4]. Further evidence of plume surface interaction directly damaging a system can be seen on *Curiosity* during the landing of MSL, which resulted in one of the rover's wind sensors being damaged by ejecta [6]. However, arguably more problematic is that PSI is hard to predict due to complex physics and limited experimental capabilities on Earth [3].

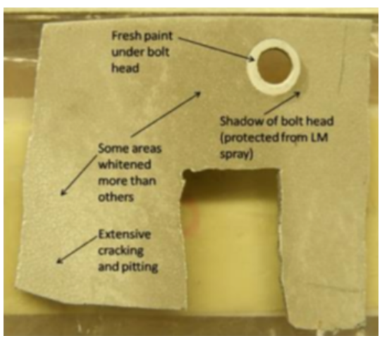

Figure 1: Evidence of sandblasting on Surveyor III's camera shroud [4].

To this point, even though estimates exist for the altitude at which lunar PSI becomes non-negligible, they are not commonly accepted, as lunar PSI depends largely on the lander itself [7, 8]. Indeed, it is possible to construct a simplistic, scalable model to predict the altitude of PSI domination and the affected lunar surface area. However, these predictions are rudimentary at best. Clearly, the production of ejecta and cratering of the lunar surface are poorly understood, hazardous phenomena that present themselves as roadblocks to a continued human presence on the Moon. As such, solutions must be presented that overcome the hurdles to their understanding and mitigation.

1.2 Solution Approach and Overview

To combat both the poor understanding of lunar PSI and the phenomena itself, AGSL has designed a deployable, autonomous, artificial landing pad (called SOLACE) to mitigate the effects of regolith dispersal and cratering. SOLACE's primary objectives are: to act as a safe landing platform for DLA systems, to reduce the impact of lunar PSI on local infrastructure, and to monitor lunar PSI on its own descent as well as for future landers, for a timespan of at least 10 years. SOLACE's secondary objective is to retain the capability to act as a foundation for future lunar infrastructure. SOLACE shall be launched from Earth aboard the Space Launch System (SLS). The SLS will deploy SOLACE into a Low Lunar Orbit (LLO). At that point, Figure 2 displays the proceeding Concept of Operations (CONOPS) for SOLACE. In the case that SOLACE becomes unable to meet its primary objectives, it will be considered “inoperable” and the CONOPS will advance to Step 6.

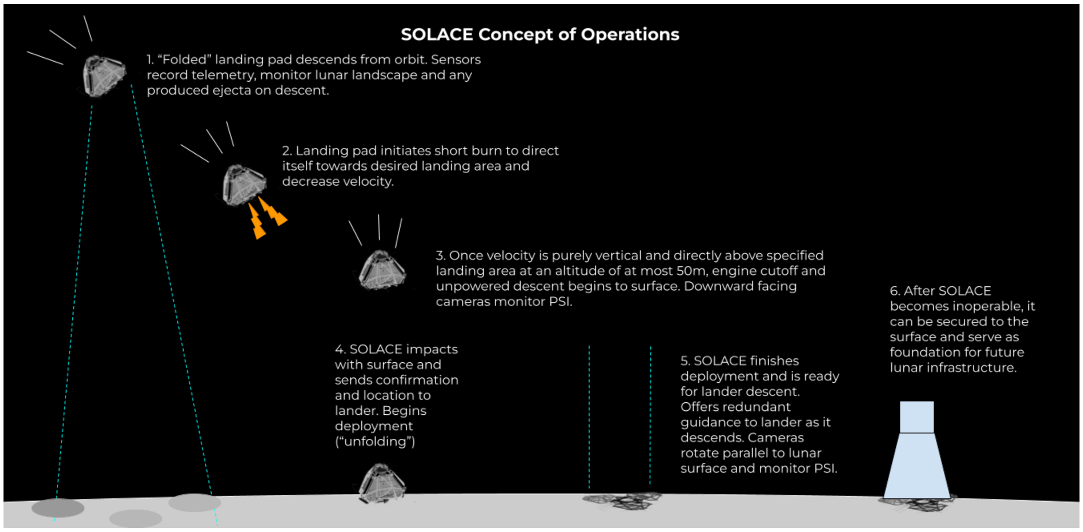

Figure 2: Concept of Operations for SOLACE, beginning from deployment in LLO.

The selected landing site for SOLACE is in the Haworth Region with latitude and longitude coordinates of (-86.50757, 342.98057). This site was selected as a part of a trade study compared to NASA’s other potential landing sites for the Artemis missions and was chosen over the others for its access to Permanently Shadowed Regions (PSRs) and low slope across the site. Figure 3 depicts the optimal landing pad landing site within the Haworth Region and Figure 4 illustrates the slope across the Haworth landing region.

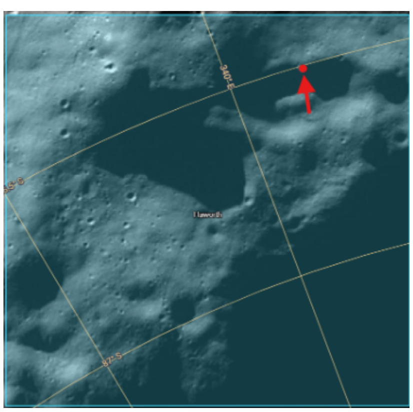

Figure 3: Optimal SOLACE landing site.

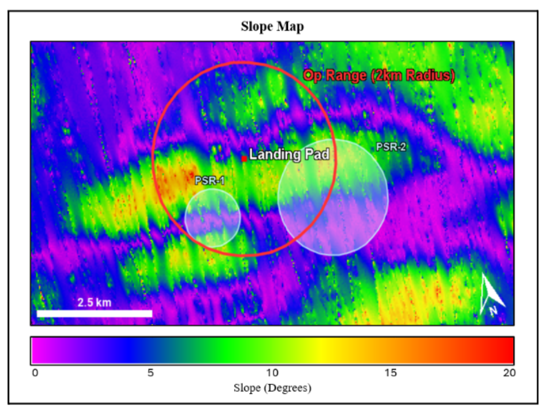

Figure 4: Slope map of the Haworth landing region.

2. SYNTHETIC ORBITAL LANDING AREA FOR CRATER ELIMINATION (SOLACE)

2.1 Post-Proposal Adjustments

Many of the post-proposal adjustments were made in response to extremely valuable criteria and insights provided by the HuLC judges at the proposal stage. These critiques involved concerns over the grating and ducting system, the survivability of the landing of a Human Landing System (HLS) vehicle, and the risk of SOLACE becoming a projectile off of the lunar surface. These concerns as well as the rest of the commentary given to the proposal will be addressed later in this paper.

Most notably, a system was added and developed to allow for SOLACE to better measure lunar PSI for itself and future landers. The elevation of SOLACE's previously secondary objective of measuring lunar PSI to primary status necessitated the inclusion of a dedicated subsystem for accomplishing this task. The elevation of this objective was done to better differentiate SOLACE from existing patents of lunar landing pads, a concern expressed by the HuLC judges. Two cameras were added to SOLACE to form a three camera suite with the navigational camera. After SOLACE completes its landing on the lunar surface, it will rotate its cameras parallel to the lunar surface. There, it will operate during future DLA system missions to track dust particles, characterizing regolith dispersal.

Another major change implemented to SOLACE is the addition of spring-actuated stakes into its landing legs. HuLC judges expressed concern from the proposal that there was a reasonable possibility that the landing pad itself would be turned into a projectile off of the lunar surface upon DLA system descent. Further technical design confirmed this and necessitated the inclusion of stakes aboard the landing pad. The addition of these stakes helps to mitigate this risk by stabilizing and securing the landing pad. Further changes to SOLACE's design include the selection of a different antenna to ensure frequency compatibility with lunar satellites, refinement of its physical model, and minor fixes done to its electrical system design.

2.2 System Design

2.2.1 Thermal, Mechanics, and Structures (TMS)

The TMS subsystem was designed to cause no harm to the lunar lander, which consists primarily of reducing heat reflection onto a given DLA system and maintaining stability on the lunar surface under intense pressurization. Additionally, the system must maintain structural integrity under extreme weight loads and temperatures while also maintaining a design that reduces and mitigates PSI. Using specifications of NASA's candidate human landers, simulations were performed to determine a maximum incident pad temperature of 3500°K and maximum weight load of 162 kN. These specific values are enumerated due to being the main design drivers of the structure.

The design that was ultimately selected and developed was a "bunker"-esque design, which is shown in Figure 5. The structure can be broken up into multiple components. The first is the lower base of the craft, which houses all electrical components, sensors, and other sensitive equipment stored on board. The second is the main plume redirection system, which redirects the DLA system's nozzle exhaust and deflects the heat in a manner that protects both the pad's systems and ground-based infrastructure outside the line of redirection. The third component is the perforated region in the center of the landing pad, which aids in the redirection of the nozzle exhaust. This area faces the most intense heat from the DLA system. The fourth and final component is the main landing surface. This component is particularly complex due to its ability to operate in a stowed and deployed configuration. It is made of 18 pieces attached to spring-loaded

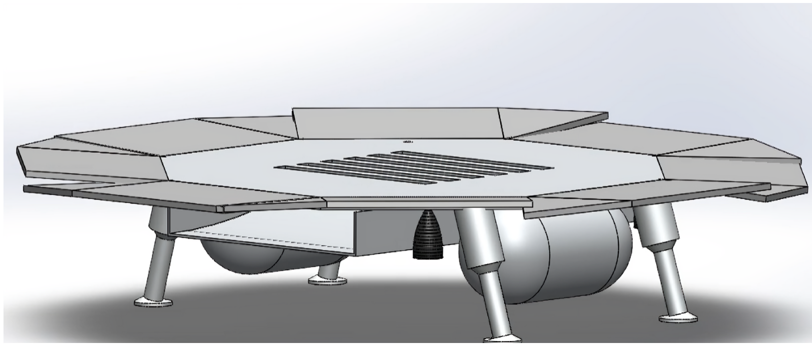

Figure 5: Deployed configuration of SOLACE.

actuators that intricately fold and deploy when commanded to do so. During structure actuation, each piece hinges according to its position on the structure and is deadbolted when an equilibrium position is reached. This equilibrium condition is achieved when the outfolding pieces are flush with the main structure. This highly complex method of deployment resulted in a number of challenges, mainly in maintaining structural stability while also accounting for the extreme temperatures that will be experienced on the lunar surface. The temperature estimate of 3500°K calls for exotic materials that not only withstand the heat without facing physical changes, but also have a low enough thermal conductivity to deflect the heat and protect the internal components of the structure. The deflected heat is sent in a direction that does not harm the lander or any nearby infrastructure.

Following an intensive materials trade study, graphene was selected as the main material for SOLACE. Graphene has an incredibly low density of 0.23 g/cm^3 [9]. This low density allows for a significant reduction in mass while also maintaining structural integrity. However, graphene was found to not withstand the intense rocket exhaust temperatures [9]. To address this, several other materials were also integrated into the design. The component of the landing pad, which houses the electrical components, uses hafnium diboride as a coat. Hafnium diboride's melting point is around 3650°K [10]. This comes at the cost of a high density of 10.3 g/cm^3 [10]. The perforated region of the craft also uses hafnium diboride. However, from thermal simulations, the nature of the heat here necessitated a significantly thicker coat than that for the "bunker" to prevent plastic deformation. The actuating part of the landing pad utilizes titanium aluminide, which offers a melting point of around 1725°K [11], an incredibly high ability to withstand loads, and a density of only 4.0 g/cm^3 [11]. This material is also used as a coat over the main graphene structure. Considering graphene's brittle nature, the structure distributes the load created by not only itself but also that of the lander, preventing buckling of any structural component.

Finally, the design includes liquid-propelled boosters. These boosters are used primarily for a controlled descent of SOLACE on the lunar surface. Moreover, these boosters are capable of flow vectoring to limit regolith dispersal on descent as well as attitude control of the craft on descent. A trade study was performed to select the fuel type for the boosters, ultimately settling on methalox as opposed to hydrazine. Hydrazine was discarded as it violates the non-toxic condition of the HuLC guidelines. In all, the dry mass of SOLACE was found to be 14.38 metric tons and the wet mass was estimated to be 25.38 metric tons. Additionally, SOLACE stands 1.4 meters tall, occupies a total volume of 18.28 m^3, and contains 9 m^3 of volume to hold other subsystems and experiments.

2.2.2 Guidance, Navigation, and Control (GNC)

The GNC subsystem is crucial for the descent and landing sequence of SOLACE. Its primary roles are to ensure that the landing pad maintains a stable orientation, slows to a safe velocity on descent, mitigates lunar PSI, and provides a safe landing sequence. In addition, the GNC subsystem is responsible for developing abort sequences that may come to be if a critical condition is reached during the descent sequence.

The navigation system revolves around an inertial measurement unit (IMU), star tracker, sun sensor, and a LiDAR sensor. Trade studies were conducted on all of these components, with important criteria being a high Technology Readiness Level (TRL) and accuracy for each component. The selected components were respectively the Honeywell HG1900 IMU, RocketLab's ST-16HV star tracker, RedWire's Coarse Sun Sensor (Cosine Type), and NASA's Navigational Doppler LiDAR (NDL). Following NDL's successful operation aboard Intuitive Machines' Nova-C lander, its TRL has improved to an acceptable level for use aboard the system.

The guidance system employs a novel machine learning-driven algorithm in tandem with on-board sensor measurements. This algorithm is performed on-board and allows the system to identify safe landing zones during descent. This algorithm is trained from available video from previous lunar missions. Due to the likelihood of dust kickup during descent, a Kalman filter is used to handle noisy measurements and allow for a smooth landing.

The control system consists of the vectored boosters provided by the TMS subsystem. These boosters are capable of both translational and angular control and, after careful analysis, sufficiently meet the GNC subsystem's objectives.

To synthesize the guidance, navigation, and control systems, a flow diagram of the GNC subsystem was developed. The flow diagram depicted in Figure 6 illustrates the step by step process performed by the GNC subsystem. It covers its performance from orbit to descent and landing in addition to the connections between the subsystem's hardware. SOLACE's descent can be split into three stages: initial descent from orbit, thrusters engaged, and final descent. Over the entire sequence, SOLACE will follow the trajectory prescribed by the guidance algorithm and will constantly evaluate its state vector to ensure nominal operation. To begin the second stage, the system will receive a signal to activate its thrusters and begin powered descent.

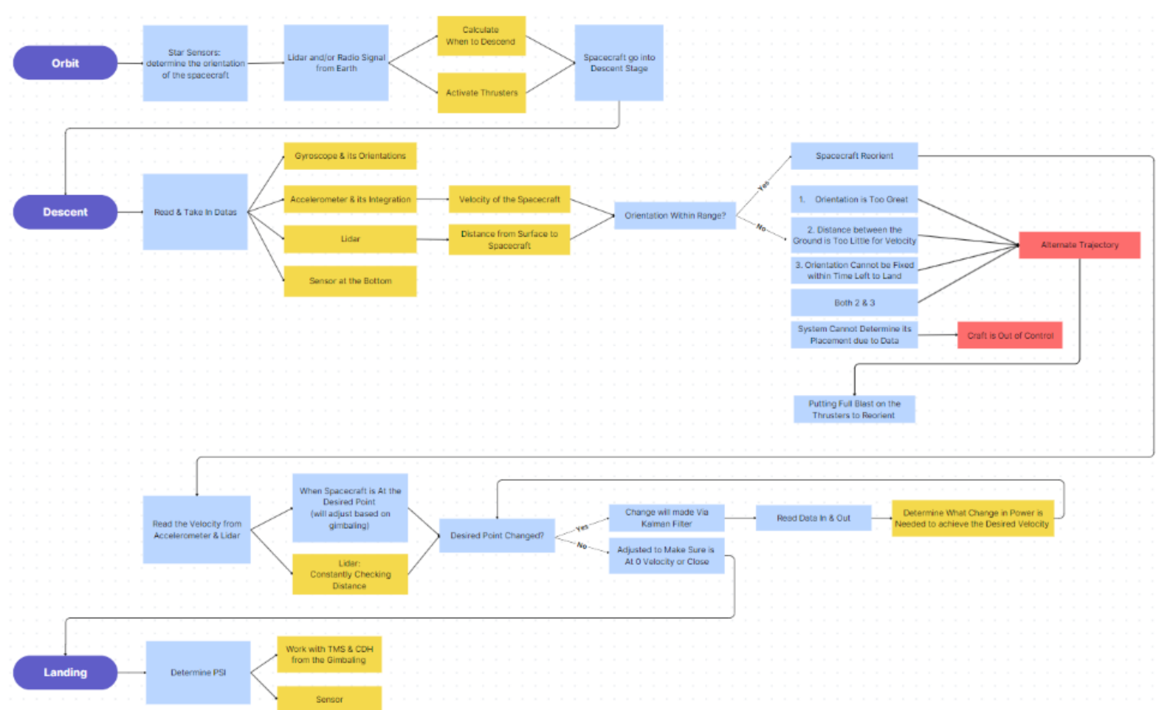

Figure 6: GNC state machine for SOLACE's descent sequence.

For the scope of this mission, SOLACE is assumed to start in LLO. During this stage, SOLACE performs a gravity-assisted descent. This is done to reduce weight that would be used for fuel necessary in a powered descent from this stage. The pad's boosters will be used for minor attitude adjustments during this stage. In the second stage of descent, which occurs at roughly 46.3 km above the lunar surface, thrusters are engaged. In concurrence with commands issued by the machine-learning-driven guidance system, the thrusters will continue to be engaged throughout this stage of descent. During the transition from descent to landing, SOLACE's downward-facing cameras will be monitoring the severity of lunar PSI. In the event of heavy PSI, the GNC subsystem will direct the boosters to vector closer to parallel with the lunar surface to reduce PSI directly beneath the landing pad. SOLACE will continue to descend until the boosters can vector no further and PSI is apparent. This altitude will be no higher than 50 meters above the lunar surface. Up to this point, SOLACE will have been slowed to 0 m/s. Here, the boosters will cut off and SOLACE will enter a free fall to the lunar surface.

To aid in system robustness and to prevent damage to the landing pad and lunar surface, the guidance algorithm was designed to retain abort trajectories in the event of departure from the commanded trajectory. The conditions for abort depend primarily on the pad's attitude. If the commanded attitude is maintained throughout descent, then the primary landing sequence will be carried out. In the case of the landing pad departing from the desired attitude, the guidance algorithm will select the abort trajectory that requires the least amount of fuel to achieve and will command the landing pad to follow that trajectory. The existence of abort options throughout the entirety of the landing sequence allows for SOLACE to minimize damage to itself and the lunar surface while achieving its primary objectives despite off-nominal scenarios.

2.2.3 Electrical Power Subsystem (EPS)

The primary objectives of the EPS are to provide power generation, storage, and management to all the entirety of the SOLACE system. SOLACE's EPS will operate on a staged layout, isolating the various components from one another based on their power requirements and their role in the overall system. Dedicated electrical buses are allocated to each subsystem to prevent overall collapse in the event of a system failure. Additionally, power requirements are separated into high and low side switching, making use of transformers to provide sufficient input power to sensitive components on the sensor array while keeping them isolated from the high current environment that the actuators are located in. This also prevents interference that the motor and solenoid's magnetic fields create from distorting the signals present in the sensor array.

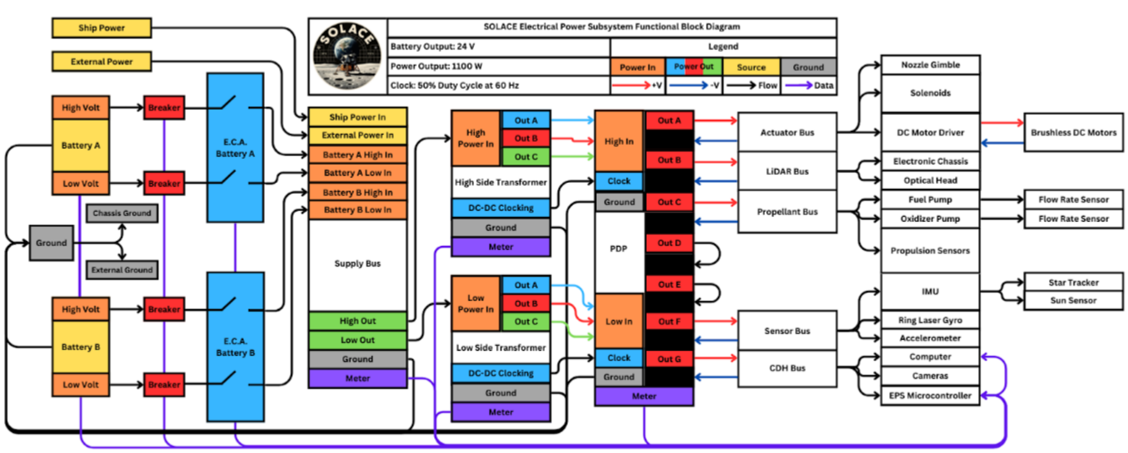

Figure 7: Block diagram for SOLACE's electrical system.

The EPS begins at the power supply where two 7-cell lithium-ion batteries are located, allocated as a high and low side supply. The electrical control system (ECS) closes the connections between the supply and the rest of the subsystem depending on the stage of flight and power draw needed. Circuit breakers protect the rest of the subsystem from unexpected surges and discrepancies between the supply and the ECS. From the ECS, power is fed into the primary supply bus where relays switch the supply between high and low outputs. Additionally, this bus has a slave port, allowing the batteries to be used to power other systems on a need-based basis, as well as an external power supply port, allowing the pad to be powered by an external source. Not only do these features provide redundancy, but they also add potential for further pad development once installed on the lunar surface. From the supply bus, power is routed into a high side bus and a low side bus. These buses utilize transformers to step up and step down voltage based on the system needs. Additionally, DC-DC clocking is used to feed pulse width modulation (PWM) for the actuating system's motor drivers. This is done by having several power converters embedded in the bus to step a dedicated supply voltage up and down to produce a clocking signal. These high and low buses then feed a primary power distribution panel, separating all supply voltages into dedicated supply lines for each subsystem. Metering is performed at each stage of the EPS to monitor system status and any discrepancies present within the EPS. All of this information is fed into a dedicated microcontroller, as well as switching signals, for the EPS and the primary computer for redundancy.

The computed power draw for the EPS is displayed in Figure 8. Missing specifications are either due to unavailable information on the selected equipment or contingent on rigorous hardware testing.

System	Component	Manufacturer	Power	Voltage	Current	Quantity
Sensor Array	Navigation Doppler Lidar	NASA Langley	80 W	28 VDC	2.857 A	1
	GG1320 Ring Laser Gyr	Honeywell	1.6 W	15 VDC	0.107 A	1
	HG1900 IMU	Honeywell	3 W	5 VDC	0.6 A	1
	Coarse Sun Sensor	RedWire	0 W	TBD	0.0013 A	1
	ST-16HV Star Tracker	RocketLab	0.5 W - 1 W	9 - 34 VDC	0.056 A (MAX)	1
	TMP64 Thermistor	Texas Instruments	0 W	5.5 VDC	0.0 A	4
	Accelerometer	NASA JPL / UCLA	0.058 W	TBD	TBD	1
Computer	Jetson AGX Orin	NVIDIA	15 - 60 W	12 VDC	5.0 A (MAX)	1
	IMX586 Camera	ArduCam	1.19 W	5 VDC	0.238 A	3
Control	PD82152B BLDC Motor	Transmotec	120 W	24 VDC	7.2 A	4
	SDU-.75 WASolenoids	Moog	10 W	24 VDC	0.42 A	16
	MCF8315C Driver	Texas Instruments	1 W	4 - 35 VDC	4.0 A	4
Propulsion	Fuel Pump	NASA Glenn	500 W	TBD	TBD	4
	Oxidizer Pump	NASA Glenn	500 W	TBD	TBD	4
	Gimble	NASA Marshall	TBD	TBD	TBD	4
Totals:			4793.228 W (MAX)			

Figure 8: SOLACE's power budget at beginning of life (BOL). [12, 13, 14, 15, 16, 17, 18]

SOLACE's EPS also includes a robust and developed sensor suite. To begin, the EPS utilizes the NDL. This radar system utilizes a laser-based sensor to deliver precise vehicle velocity vector and altitude information crucial for navigation and landing within autonomous GNC systems. This system operates by emitting three laser beams in fixed directions, enabling calculation of velocity and range along the laser's line of sight without requiring altitude angle data. Consequently, altitude measurements are obtained simultaneously with velocity vector data, eliminating the necessity for additional sensors. The system's construction is comprised by the laser, receiver, local power distribution unit (PDU), controller, and signal processor, while the optical head incorporates three lenses for data collection. Transmission of data from the optical head to the chassis occurs through a fiber optic cable. Noteworthy advantages include its lightweight, compact design, and high precision in data collection. However, drawbacks include a relatively high power draw of 80W and susceptibility of delicate parts to vibrations, necessitating careful handling.

Additionally, the EPS employs a ring laser gyro for attitude determination. This gyro operates by employing a pair of laser beams traveling in opposing directions to measure rotation rates of an object utilizing the Sagnac effect. As these beams traverse their paths, meeting points are generated, producing an interference pattern pivotal for calculating rotation rates and attitude. Conceptually, two beams emanate from a common point, traversing opposite directions around a closed loop of reflectors typically arranged in a triangular or square configuration. Upon reconvergence, any disparity caused by alterations in motion results in a detectable shift in the interference pattern, facilitating the calculation of rotation rates and attitude. The system's construction entails a closed-loop configuration, comprising a beam transmitter, reflectors, and a detector situated at the starting point to receive the returning beams. Despite being extensively utilized across various aerospace applications, offering high precision and data rates alongside reliability within a compact design, the system has its drawbacks. These include the "lock-in" effect, where the beams interface with each other, susceptibility to temperature fluctuations, vibrations, and other stressors, as well as a notable high cost factor.

An accelerometer is included for determination of the pad's translational acceleration. Inside the accelerometer, a proof mass is suspended by springs, and when the structure experiences acceleration, the proof mass moves relative to the accelerometer's frame. This movement generates a change in capacitance, piezoelectric effect, or other measurable physical phenomenon, which is then converted into an electrical signal proportional to the acceleration. The signal is then processed on-board an interpreted for the use in GNC systems.

A thermistor is employed to measure temperature variations in critical components and propulsion systems to ensure operational stability in extreme conditions. Linear thermistors offer linearity and consistent sensitivity across temperatures to enable simple and accurate methods for temperature conversion. Lower power consumption and a small thermal mass minimize the impact of self-heating. With built-in failsafe behavior at high temperatures and powerful immunity to environmental variation, these devices are designed for a long lifetime of high performance. The small size of the TMP6 series also allows for close placement to heat sources and quick response times. The sensor suite also includes the aforementioned Redwire Coarse Sun Sensor (CSS) Pyramid and the ST-16HV Star Tracker. These are included for relative attitude determination of the landing pad.

Finally, the EPS employs various actuators to accomplish its objectives, namely brushless DC (BLDC) motors, solenoids, and driver. The BLDC motors employed by SOLACE are used primarily for the leveling of the landing pad. As such, the motors are only expected to move a small distance, but are strong enough to support both the weight of the pad and any supported DLA system. The solenoids aboard SOLACE were selected to be Moog's SDU-.75 WA solenoids. The SDU-.75 WA solenoids would be used to trigger the spring-loaded panels on the landing pad. The solenoids are strong enough to hold the force of the springs down until the pad reaches the stage of flight necessary for panel deployment. In this manner, these solenoids act as locks against panel deployment. The drivers aboard the pad help convert PWM signals, produced by the DC-DC clocking, into efficient signals for the motors to operate at. The Texas Instruments MCF8316C driver provides the necessary input and output power requirements to support BLDC motors at SOLACE's scale.

2.2.4 Communications (COM)

The main objective of the COM subsystem is to ensure that a stable communications link is maintained between SOLACE and an arriving vehicle. To do this, several trade studies were conducted on the antenna, transceiver, transmitter, and communication schemes to be employed on-board.

The transceiver chosen was the SRS-4 Full-duplex High-Speed S-band transceiver. The transceiver operates on the ITU approved S-band frequencies. The center frequency of our design and simulations was chosen to be 2250 MHz. The modulation method is 16-QPSK along with CCSDS compatible channel coding. This channel coding enables the system to be compatible with independent and commercial ground station networks. The system has a variable transmit symbol rate up to 10 MB/s. The system also communicates with the CDH subsystem's NVIDIA Jetson Nano board by RS-422 with a bitrate up to 12.5 MB/s. The system uses standard Forward Error Correction (FEC) to achieve its desired bit error rates (BER). Checksum CRC, Reed-Soloman, and convolutional forward error control coding are also used to achieve the desired transmission rate of 10MB/s and acceptable BERs.

The communication link of our system took into account the normal parameters of a telecommunication system design along with our mission specific parameters regarding the lunar surface. The transmitter average power output is set to be 4W with a transceiver antenna gain of 9 dBi, with a maximum gain of 11 dBi. Key mission-specific discoveries were made in relation to the effect of lunar regolith and terrain on our transmitted signal. The lunar regolith permittivity was deemed to be 3 F/m and the conductivity as 10E-14 S/m in sunlight, while 10E-9 in darkness. Diffraction and reflection of the S-band frequencies had a mitigated effect on the composition of the signals as well. Research showed the diffraction and reflection attenuation is much more prevalent at lower frequencies (250 MHz) compared to S-band frequencies (2.4 GHz). This can be seen in changes in the antenna radiation patterns. The lunar ground acts as a partial reflector and absorber in much greater effect at frequencies below the S-band. Therefore, it is estimated that only a 5-10 dB loss is necessary to be accounted for in conjunction with the free space path loss for S-band frequencies.

The selected antenna was the IQ-Spacecom S-band patch antenna. This antenna is able to operate on the intended center frequency of 2250 MHz, has a maximum gain of 11 dBi, is circular polarized for transmitting and receiving, and has a bandwidth of 50 MHz. The passive antenna is able to operate with the SRS-4 transceiver by means of a simple RF cable. All calculations and conclusions from above were determined using MATLAB's Communications Toolbox.

2.2.5 *Command and Data Handling (CDH)*

The CDH subsystem is crucial for the seamless execution and management of SOLACE's mission timeline. Its primary role is to implement a hierarchical state machine (HSM) that adeptly coordinates the responses of various subsystems to dynamic mission events. In addition, the CDH team is responsible for the creation of an algorithm to monitor PSI and particle dynamics over the duration of SOLACE's lifetime. The CDH subsystem performed several trade studies to select and develop the necessary hardware to accomplish its objectives. Namely, this consists of choosing a flight computer and cameras aboard SOLACE. For the flight computer, the need to handle several complex algorithms necessitated the selection of the NVIDIA Jetson Orin AGX 64 GB Developer Kit. For the purposes of monitoring PSI, three ArduCam IMX586 48MP Camera Modules were elected to be used.

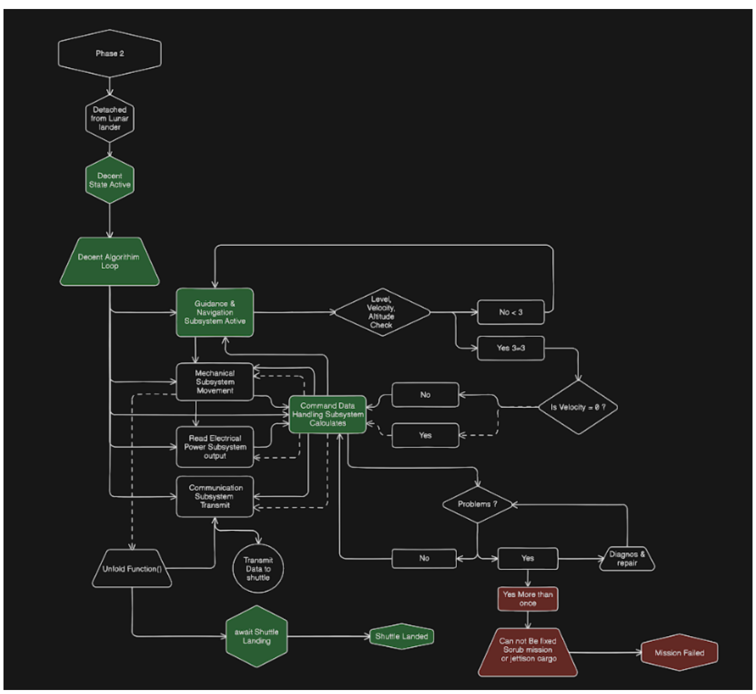

Figure 9: In-flight HSM for SOLACE's CDH subsystem.

In the environment of lunar development, where multiple subsystems operate under varying and unpredictable conditions, a robust management system is required to ensure the optimal operation of the system. The large collection of subsystems reacting to asynchronous and nondeterministic inputs creates a control problem that is best solved by an HSM. The HSM provides a structured, yet flexible management framework that effectively reduces the complexities involved in the subsystem interactions [19]. The hierarchical organization of states allows for a modular design, where states are nested within each other, simplifying the control logic and reducing redundancy. This is crucial for preventing exponential increases in complexity. This prevents the common "exploding" problem of Finite State Machines (FSM) in which the complexity of the solution scales exponentially with the complexity of the problem [20]. The orthogonality achieves concurrency, which is essential in a machine consisting of many subsystems. This is in opposition to FSMs, which are less adept at managing the high complexity and asynchronous nature of space mission controls, as each new state multiplies the number of transitions and interactions needed to be managed.

SOLACE's HSM focuses on creating states centered around the pre-planned phases of the mission. These events help the HSM define what nominal operations should be at set points in the mission. As a result, this allows the HSM to ensure mission success. Pre-flight and mid-flight checks help ensure that all systems are nominal before and during flight. Orbital assurance checks allow for the fine-tuning of SOLACE's trajectory and orientation to ensure lunar insertion. Active descent and error management capabilities enable the handling of real-time adjustments and anomalies during lunar descent. With these checks, the HSM could be properly developed for all mission phases: pre-flight, in-flight, and post-flight operations. Displayed in Figure 9 is the HSM for SOLACE's in-flight phase.

Additionally, due to the elevation of PSI measurement and monitoring to a primary objective, the formulation of a way to measure PSI was deemed necessary. The characterization of lunar PSI is done by having the on-board cameras observe and record the effects of lunar PSI, namely regolith dispersal. To do so, the CDH subsystem elected to use 3D particle tracking velocimetry on regolith particles larger than 20μm. Doing so allows the CDH subsystem to track the size and velocity of significant regolith particles, allowing for better development of current PSI models. Figure 10 displays the flow diagram of the implemented PSI characterization algorithm.

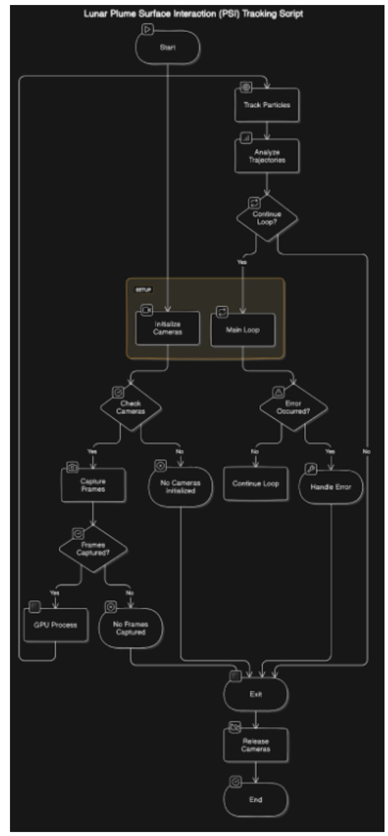

Figure 10: Algorithm for on-board particle tracking.

2.2.6 *Verification and Validation (VV)*

In addition to a robust design, a unique verification and validation (VV) plan was developed for each subsystem. The TMS and EPS subsystems follow standard VV plans, while GNC, COM, and CDH follow an Adaptive Independent VV plan. The Adaptive Independent VV plan utilizes the agile task management method for efficient assurance of system performance.

Per SOLACE's proposal, the VV plan for TMS consisted of constructing a small-scale prototype of the landing pad and subjecting it to conditions similar to that on the lunar surface. Due to the exclusivity of hafnium diboride, it was unfeasible to acquire to integrate into the physical model. This prevented the testing of extreme temperatures on the small-scale prototype. However, other tests, such as a drop test, stability tests, vibration testing, and simulated Moon quakes were performed and passed. The physical prototype is shown in Figure 11.

The GNC subsystem was able to both verify and validate its system via a combination of Python scripts and NASA'S General Mission Analysis Toolkit (GMAT) software. Using a script for the aforementioned descent sequence, a landing scenario was simulated in GMAT. The trajectory is illustrated in

Figure 12 and indeed shows a successful descent of SOLACE to the lunar surface. An accompanying plot in Python, Figure 13, was generated displaying SOLACE's speed as it descends down to the lunar surface. In this plot, the second stage of the descent is modelled as an impulsive burn for simplicity. As a result of these simulations, the GNC subsystem functions as designed, achieving its primary objectives.

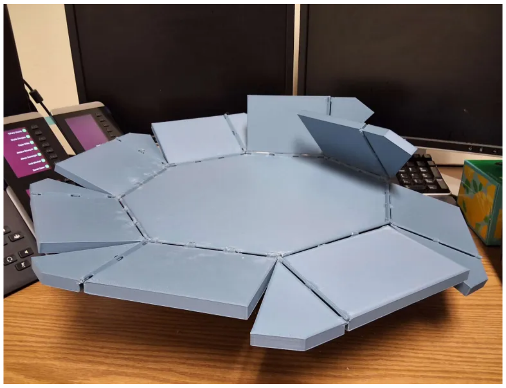

Figure 11: 3D-printed model that was tested for VV of TMS.

For the EPS subsystem, its VV plan consisted of ensuring that power could be stored and distributed properly aboard the landing pad. This was done by building a small-scale EPS-specific prototype. This prototype consisted of a deployable fin, temperature sensor, accelerometer, and distance sensor controlled by an Arduino Raspberry Pi. Ultimately, the prototype was able to verify and validate that the EPS could manage pad deployment on command as well as an integrated sensor suite, fulfilling its primary objectives.

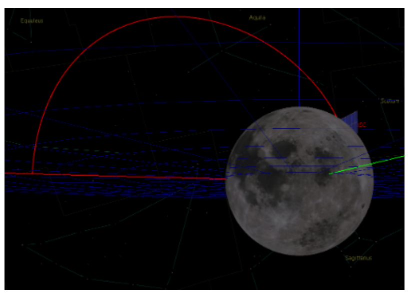

Figure 12: GMAT simulation of SOLACE's descent.

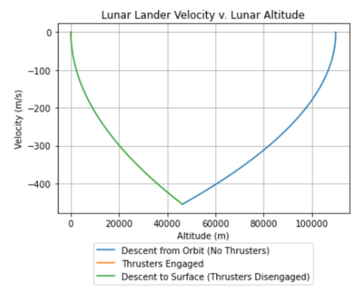

Figure 13: Velocity magnitude of SOLACE during descent.

The COM subsystem's VV plan consisted of frequency testing, data rate transmission and spectrum efficiency testing, encryption testing, and pad to Earth communication testing. A simulated test environment was set up inside of MATLAB's Communications Toolbox, where the selected design components and parameters were used to analyze these properties. As a result, a link budget was formulated, producing an average receiver power of -44.18 dBi, meeting the COM subsystem's requirements and fulfilling its primary objectives.

Finally, the VV plan for the CDH subsystem was determined to be based on the response of the subsystem to various errors analyzed by isolated testing of subcomponents. The CDH subsystem was able to complete this task by the creation and testing of flight software aboard the EPS prototype. Unit testing of the fin deployment and each sensor in the model allowed the CDH subsystem to verify their state machine's robustness against errors.

2.3 System Merit

2.3.1 Performance and Adherence to Constraints

Clearly, it can be seen from the system verification and validation that SOLACE has the ability to meet its primary objectives of mitigating and understanding PSI. However, SOLACE offers specific system performance advantages that make it unique. To begin, the elected landing site in the Haworth landing region also acts as a representative for a landing region that might be selected for future lunar habitation. To this point,

Figure 14 displays the location of potential habitation zones in relation to the selected landing site. The close proximity of SOLACE's landing region to potential zones of habitation not only ensures that SOLACE will not be obstructed by the lunar surface, but also that SOLACE can meet its mission objectives in an area that is extremely relevant to NASA's goals for the present and future of lunar operations.

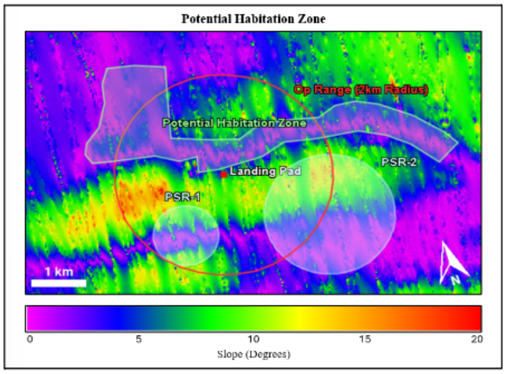

Figure 14: Proximity of SOLACE's landing site to potential habitation zones.

Focusing on SOLACE as a system, SOLACE's ability to mitigate PSI and thus, safely usher future crewed missions to the Moon, directly supports NASA's Level 0 goal of expanding human space operations on the moon for sustained lunar activities [21]. Moreover, SOLACE acts as a stepping stone towards NASA's future goals of supporting lunar infrastructure through its extended lifespan, its capability to double as an infrastructure foundation, and the fact that its landing site is representative of one recommended for lunar habitation and near areas of scientific interest.

Additionally, SOLACE offers a non-invasive solution to the problem of mitigating and understanding lunar PSI. That is, SOLACE does not damage the lunar surface and seeks to reduce the pollution of the lunar surface in its own design, by still being of use after its primary mission has ended.

Finally, SOLACE adheres to the design constraints held by NASA in its HuLC. First, SOLACE is capable of mission success in the harsh lunar environment. Its physical design was driven by the need to survive the extreme temperatures of the lunar environment. The combination of the machine learning-driven guidance algorithm with the Kalman filter helps SOLACE resiliently operate in a hectic descent environment amid expected dust kickup. The design choice of changing the selection of SOLACE's antenna frequency allows it to effectively communicate with Tracking and Data Relay Satellites (TDRSS), including but not contingent upon Gateway. Resilient design also appears in the CDH subsystem design, where the HSM consistently checks at vulnerable mission points if the pad is operating in a nominal state, and if it isn't, corrects it.

SOLACE's design hinges upon no preexisting lunar infrastructure. However, if preexisting infrastructure is developed either on the lunar surface or in orbit, then it will only go to enhance SOLACE's ability to accomplish its objectives. SOLACE requires only one landing and can handle any currently considered HLS. No additional risks are posed to the crew as a result of several risk mitigation strategies taken by SOLACE. The SOLACE was also careful to use non-toxic solutions, being the design motivator behind switching from hydrazine propellant to methalox. While the scalability of SOLACE for HLS is a founded concern, positive results from conducted simulations on the loading and stability of the physical prototype lend credence to the fact that SOLACE can be scaled to meet this concern, supporting its candidacy as a 3-5 year solution. However, it should be said that further testing should be conducted on a more representative model, which comes with a larger prototyping budget.

2.3.2 Technology Readiness

Most of the technology that is used aboard SOLACE has been mission-proven and is considered of TRL 9. Being the case, this allows more resources to be allocated towards the building, integration, and testing of SOLACE, as opposed to continuously testing new technology to raise it to an acceptable TRL.

2.3.3 *Risk*

Overall, SOLACE is a low risk solution. To begin, landing pads are low in complexity and highly common, in opposition to several other space-based technologies proposed for establishing a long term presence on the lunar surface. The high TRL of its components motivates confidence in the un-likelihood of component failure during flight. This is not to say that SOLACE is without risk. In Figure 15, five risks of high magnitude were tabulated. Numbered 1 to 5, they are: SOLACE becomes a projectile off of the lunar surface, SOLACE experiences accelerated material degradation, SOLACE's deploy mechanism fails, SOLACE experiences a brownout on descent, and SOLACE departs from its guided trajectory. The mitigation plans for these risks drove the inclusion of stakes to secure SOLACE to the lunar surface, selection of titanium aluminide as the main structure material, use of spring-loaded actuators for deployment, robust regulation of SOLACE's electronics, and intelligent abort sequences along with adjustments at vulnerable mission points over the mission duration. These allowed the risks to be moved to 1f-5f respectively.

Figure 15: Response of SOLACE's risks to implemented mitigation strategies.

2.3.4 *Programmatic Implementation*

SOLACE also offers many advantages in the sense of programmatic implementation. These advantages all coalesce into the benefit that SOLACE can be used for a variety of missions and scenarios. SOLACE is designed to be compatible with any chosen HLS vehicle. Additionally, SOLACE was also designed to work in a variety of lunar regions. Its leveling capability allows it and selected HLS vehicles to operate in zones of higher slope, which might have been previously inoperable.

2.4 System Costing and Scheduling

2.4.1 *Cost Estimation, Budget, and Affordability*

For the cost estimation of SOLACE, NASA's Project Cost Estimating Capability (PCEC) software was used. NASA's PCEC uses design parameters of a system in tandem with previous missions to produce a cost estimate for each item in a work breakdown structure (WBS) [22]. Using this tool, Figure 16 was developed, which displays the total cost breakdown of the entirety of a SOLACE mission. Specific items of note are a non-recurring cost (NRC) for the spacecraft of \$168.1M FY2024, a total flight system cost of \$1,000.9M FY 2024, and a total program cost of \$1,944.9M FY 2024.

Synthetic Orbital Landing Area for Crater Elimination (SOLACE) Lifetime Cost Estimation

Units Conversion Factor: 1.000

FY2024 $M   Inflation Factor: 1.187

WBS #	Level	Line Item Name/Description	Non-Recurring	Design & Development	System Test Hardware	Flight Unit	Recurring Production	Non-Allocated	Operations	TOTAL	Fee + Burden	TOTAL w/Fee + Burden
0	1	System Name	$ 290.5	$ -	$ -	$ -	$ 1,051.8	$ 232.4	$ 370.2	$ 1,944.9	$ -	$ 1,944.9
1.0	2	Project Management	$ 19.1	$ -	$ -	$ -	$ 44.4	$ -	$ -	$ 63.5	$ -	$ 63.5
2.0	2	Systems Engineering	$ 10.6	$ -	$ -	$ -	$ 17.1	$ -	$ -	$ 27.6	$ -	$ 27.6
3.0	2	Safety and Mission Assurance	$ 15.5	$ -	$ -	$ -	$ 34.0	$ -	$ -	$ 49.5	$ -	$ 49.5
4.0	2	Science/Technology	$ -	$ -	$ -	$ -	$ -	$ 42.6	$ -	$ 42.6	$ -	$ 42.6
5.0	2	Payload(s)	$ 7.1	$ -	$ -	$ -	$ 15.6	$ -	$ -	$ 22.7	$ -	$ 22.7
5.01	3	Payload Management	$ 2.5	$ -	$ -	$ -	$ 5.8	$ -	$ -	$ 8.3	$ -	$ 8.3
5.02	3	Payload System Engineering	$ 0.8	$ -	$ -	$ -	$ 1.3	$ -	$ -	$ 2.1	$ -	$ 2.1
5.03	3	Payload Product Assurance	$ 0.3	$ -	$ -	$ -	$ 0.8	$ -	$ -	$ 1.1	$ -	$ 1.1
5.10	3	Instruments - EMPTY ROLLUP	$ -	$ -	$ -	$ -	$ -	$ -	$ -	$ -	$ -	$ -
5.x	3	Payload I&T	$ 3.5	$ -	$ -	$ -	$ 7.7	$ -	$ -	$ 11.2	$ -	$ 11.2
6.0	2	Flight System \ Spacecraft	$ 190.3	$ -	$ -	$ -	$ 810.6	$ -	$ -	$ 1,000.9	$ -	$ 1,000.9
6.01	3	Flight System Project Management	$ 1.0	$ -	$ -	$ -	$ 2.3	$ -	$ -	$ 3.3	$ -	$ 3.3
6.02	3	Flight System Systems Engineering	$ 1.8	$ -	$ -	$ -	$ 2.9	$ -	$ -	$ 4.7	$ -	$ 4.7
6.03	3	Flight System Product Assurance	$ 4.6	$ -	$ -	$ -	$ 10.0	$ -	$ -	$ 14.6	$ -	$ 14.6
6.10	3	Spacecraft	$ 168.1	$ -	$ -	$ -	$ 762.6	$ -	$ -	$ 930.7	$ -	$ 930.7
--	4	Structures & Mechanisms	$ 18.0	$ -	$ -	$ -	$ 670.3	$ -	$ -	$ 688.3	$ -	$ 688.3
--	4	Thermal Control	$ 0.1	$ -	$ -	$ -	$ 0.0	$ -	$ -	$ 0.1	$ -	$ 0.1
--	4	Electrical Power & Distribution	$ 1.4	$ -	$ -	$ -	$ 1.1	$ -	$ -	$ 2.5	$ -	$ 2.5
--	4	GN&C	$ 0.5	$ -	$ -	$ -	$ 0.7	$ -	$ -	$ 1.2	$ -	$ 1.2
--	4	Propulsion	$ 142.2	$ -	$ -	$ -	$ 84.4	$ -	$ -	$ 226.6	$ -	$ 226.6
--	4	Communications	$ 0.9	$ -	$ -	$ -	$ 1.2	$ -	$ -	$ 2.1	$ -	$ 2.1
--	4	C&DH	$ 5.0	$ -	$ -	$ -	$ 4.9	$ -	$ -	$ 9.9	$ -	$ 9.9
6.x	3	Flight System I&T	$ 14.9	$ -	$ -	$ -	$ 32.8	$ -	$ -	$ 47.6	$ -	$ 47.6
7.0	2	Mission Operations System (MOS)	$ 19.2	$ -	$ -	$ -	$ 66.9	$ -	$ 370.2	$ 456.3	$ -	$ 456.3
--	3	MOS/GDS Development (Phase B-D)	$ 19.2	$ -	$ -	$ -	$ 66.9	$ -	$ -	$ 86.1	$ -	$ 86.1
--	3	Mission Ops & Data Analysis (Phase E)	$ -	$ -	$ -	$ -	$ -	$ -	$ 370.2	$ 370.2	$ -	$ 370.2
8.0	2	Launch Vehicle/Services	$ -	$ -	$ -	$ -	$ -	$ 189.9	$ -	$ 189.9	$ -	$ 189.9
9.0	2	Ground Data System (GDS)	$ -	$ -	$ -	$ -	$ -	$ -	$ -	$ -	$ -	$ -
10.0	2	System Integration, Assembly, Test & Check Out	$ 28.7	$ -	$ -	$ -	$ 63.3	$ -	$ -	$ 91.9	$ -	$ 91.9
11.0	2	Education & Public Outreach	$ -	$ -	$ -	$ -	$ -	$ -	$ -	$ -	$ -	$ -

	Reserves %	TOTAL w/Reserves	TOTAL w/Fees, Burdens, &
Reserves	0%	$ 1,944.9	$ 1,944.9

Figure 16: SOLACE's total program cost breakdown using NASA's PCEC.

2.4.2 *Project Schedule and Major Milestones*

The project schedule for SOLACE involving its design, test, evaluation (DTE), and flight from the procurement of components is displayed in Figure 17. In 4.5 years, this timeline will bring SOLACE from concept to prepared for spaceflight. ET in the table below stands for elapsed time since the beginning of the DTE process.

Milestone	ET (YY:MM:DD)	Milestone	ET (YY:MM:DD)
Components Procurement	00:00:00	Environmental Testing	02:06:00
Sensor Testing	00:03:00	Subsystem V&V	03:04:00
Structure Assembly	01:00:00	System V&V	04:02:00
Structure Testing	01:03:00	Day in the Life Testing	04:02:15
EPS/CDH/GNC/COM Assembly and Integration	02:00:00	Launch Preparation	04:05:00
EPS/CDH/GNC/COM Testing	02:03:00	Flight	04:06:00

Figure 17: Major milestones in the DTE timeline for SOLACE.

3. FUTURE RECOMMENDATIONS

During the process of designing SOLACE, from the definition of system requirements to the final VV tests being performed, many takeaways were found that would be useful in the future design of systems for the expressed purpose of mitigating and understanding lunar PSI.

From an organizational standpoint, AGSL employed the use of several subteams, including TMS, GNC, EPS, COM, and CDH. However, AGSL also formed the Surface, Integration, and Test Environment (SITE) subteam. This subteam was responsible for the analysis of the lunar surface, study of regolith, and integral in the development of test procedures for SOLACE's other subsystems. The SITE subteam worked closely with each of the other subsystems to ensure that their subsystem was compatible with the lunar environment, other subsystems, and actively helped to prevent lunar PSI. This organization was extremely useful in efficient design constraint adherence, proactive subsystem design, and tackling the poorly understood issue of lunar PSI. Though it is recognized that other designs for mitigating and monitoring lunar PSI will differ in both organization, design, and implementation, AGSL recommends that large, future projects employ a similar organization, specifically with the inclusion of a SITE-adjacent subteam.

From a design standpoint, there were some aspects of SOLACE that could have been improved upon, but the team lacked the time and/or resources to. One is the design of the grating and ducting on SOLACE. During the design, flow modeling found that the grating would impede the nozzle exhaust due to the stagnation pressure above the grating bars and the exhaust gas viscosity between the bars. The SOLACE team recognized that structure optimization of the grating and ducting system would have to be performed in conjunction with further aerodynamic testing. Future projects attempting a similar design should plan to iterate several times on this design feature in particular. Additionally, as evident in Figure 16, much of the cost for SOLACE is derived from the propulsion system, both in the monetary and design senses. The propulsion system creates large temperature gradients aboard the landing pad and adds on over 3000 kg of mass. Early in SOLACE's development, the idea of it descending in an unpowered or low-powered way to the lunar surface was proposed, but discarded due to no acceptable solutions arising. If a future project designed a similar vehicle to perform a low-powered descent, it would drastically reduce the mass, volume, and cost of the structure, possibly accelerating its timeline for implementation to well under five years.

Nevertheless, AGSL would like to extend its utmost appreciation towards the NIA, NASA, and their sponsors for the opportunity to technically develop such an interesting and unique concept in SOLACE. AGSL would also like to recognize the invaluable oversight of her principal investigator, Dr. Helen Reed, and the ever-present guidance of her former program manager, Alexander Duffy, and her current program manager, Shirish Pandam. Finally, AGSL thanks Texas A&M University for its dedication to space research, phenomenal education, and continued support of student-led organizations like AGSL.

REFERENCES

[1] NIA, "Mitigating Lunar Plume Surface Interaction (PSI) 2024 Proposal Guidelines," 2023.

[2] C. Immer, J. Lane, P. Metzger, and S. Clements, "Apollo Video Photogrammetry Estimation of Plume Impingement Effects," Icarus, vol. 214, p. 46–52, 01 2014.

[3] P. T. Metzger, J. Smith, and J. E. Lane, "Phenomenology of Soil Erosion due to Rocket Exhaust on the Moon and the Mauna Kea Lunar Test Site," Journal of Geophysical Research: Planets, vol. 116, no. E6, 2011.

[4] P. Zanon, M. Dunn, and G. Brooks, "Current Lunar Dust Mitigation Techniques and Future Directions," Acta Astronautica, vol. 213, pp. 627–644, 2023.

[5] J. R. Gaier, "The Effects of Lunar Dust on EVA Systems During the Apollo Missions," Tech. Rep. NASA/TM—2005-213610, Glenn Research Center, Cleveland, OH, Mar. 2005.

[6] J. Gómez-Elvira, C. Armiens, I. Carrasco, M. Genzer, F. Gómez, R. Haberle, V. E. Hamilton, A.-M. Harri, H. Kahanpää, O. Kemppinen, A. Lepinette, J. Martín Soler, J. Martín-Torres, J. Martínez-Frías, M. Mischna, L. Mora, S. Navarro, C. Newman, M. A. de Pablo, V. Peinado, J. Polkko, S. C. R. Rafkin, M. Ramos, N. O. Rennó, M. Richardson, J. A. Rodríguez-Manfredi, J. J. Romeral Planelló, E. Sebastián, M. de la Torre Juárez, J. Torres, R. Urquí, A. R. Vasavada, J. Verdasca, and M.-P. Zorzano, "Curiosity's Rover Environmental Monitoring Station: Overview of the First 100 Sols," Journal of Geophysical Research: Planets, vol. 119, p. 1680–1688, July 2014.

[7] R. N. Watkins, P. T. Metzger, M. Mehta, D. Han, P. Prem, L. Sibille, A. Dove, B. Jolliff, D. P. Moriarty, D. C. Barker, E. Patrick, M. Kuhns, and M. Laine, "Understanding and Mitigating Plume Effects During Powered Descents on the Moon and Mars," 2021.

[8] R. Clegg-Watkins, B. Jolliff, A. Boyd, M. Robinson, R. Wagner, J. Stopar, J. Plescia, and E. Speyerer, "Photometric Characterization of the Chang'e-3 Landing Site Using LROC NAC Images," Icarus, vol. 273, p. 84–95, July 2016.

[9] C. Soldano, A. Mahmood, and E. Dujardin, "Production, Properties and Potential of Graphene," Carbon, vol. 48, p. 2127–2150, July 2010.

[10] M. Gasch, D. Ellerby, E. Irby, S. Beckman, M. Gusman, and S. Johnson, "Processing, Properties and Arc Jet Oxidation of Hafnium Diboride/Silicon Carbide Ultra High Temperature Ceramics," Journal of Materials Science, vol. 39, pp. 5925–5937, 2004.

[11] D. Dimiduk, “Gamma Titanium Aluminide Alloys—an Assessment within the Competition of Aerospace Structural Materials,” Materials Science and Engineering: A, vol. 263, no. 2, pp. 281–288, 1999.

[12] ArduCam, “IMX586 48MP USB 3.0 Camera Module Datasheet,” 2023.

[13] RocketLab, “ST-16HV Star Tracker Datasheet,” 2023.

[14] C. W. Wong and J. F. Flores, eds., SmallSat Technology Partnerships (STP) Technology Exposition, A High-Precision Continuous-Time Positioning-Navigation-Timing (PNT) Compact Module for the LunaNet Small Spacecraft, NASA JPL, 2022.

[15] T. Instruments, “Linear Thermistor with 0402 and 0603 Package Options Datasheet,” 2020.

[16] T. Instruments, “Sensorless Field Oriented Control (FOC) Integrated FET BLDC Driver Datasheet,” 2024.

[17] RedWire, “Coarse Sun Sensor Pyramid Spec Sheet,” 2021.

[18] L. S. Karumbunathan, “NVIDIA Jetson AGX Orin Series: A Giant Leap Forward for Robotics and Edge AI Applications, Technical Brief,” 2022.

[19] R. Alur, S. Kannan, and M. Yannakakis, Communicating Hierarchical State Machines, p. 169–178. Springer Berlin Heidelberg, 1999.

[20] Y. Brave, “Control of Discrete Event Systems Modeled as Hierarchical State Machines,” IEEE Transactions on Automatic Control, vol. 38, no. 12, p. 1803–1819, 1993.

[21] NASA, “NASA’s Plan for Sustained Lunar Exploration and Development,” tech. rep., NASA, aug 2020.

[22] A. Prince, B. Alford, B. Boswell, M. Pitlyk, and M. Pedigo, eds., NASA Carpe Diem, Development of a Project Cost Estimating Capability, NASA, 2014.